PAPER
Samuel M. Felton *et al.*
Self-folding with shape memory composites

1744-683X(2013)9:32;1-3

PAPER

Self-folding with shape memory composites†

Samuel M. Felton,*[a] Michael T. Tolley,[a] ByungHyun Shin,[a] Cagdas D. Onal,[b] Erik D. Demaine,[c] Daniela Rus[c] and Robert J. Wood[a]

Origami-inspired manufacturing can produce complex structures and machines by folding two-dimensional composites into three-dimensional structures. This fabrication technique is potentially less expensive, faster, and easier to transport than more traditional machining methods, including 3-D printing. Self-folding enhances this method by minimizing the manual labor involved in folding, allowing for complex geometries and enabling remote or automated assembly. This paper demonstrates a novel method of self-folding hinges using shape memory polymers (SMPs), paper, and resistive circuits to achieve localized and individually addressable folding at low cost. A model for the torque exerted by these composites was developed and validated against experimental data, in order to determine design rules for selecting materials and designing hinges. Torque was shown to increase with SMP thickness, resistive circuit width, and supplied electrical current. This technique was shown to be capable of complex geometries, as well as locking assemblies with sequential folds. Its functionality and low cost make it an ideal basis for a new type of printable manufacturing based on two-dimensional fabrication techniques.

1 Introduction

There is a growing interest in developing manufacturing methods that are inexpensive, modular, and require minimal capital investment or engineering expertise. We refer to this class of techniques as *printable manufacturing* because of the ability to quickly turn digital plans into physical objects. We believe this synthesis will revolutionize manufacturing by encouraging open-source hardware, end-user fabrication, and rapid prototyping. Currently, 3-D printing–depositing material directly into a desired structure – is the most common method of this type.[1–3] However, an origami-inspired technique has recently been demonstrated that creates three-dimensional structures by folding two-dimensional materials.[4–6] This has several advantages over traditional methods: folding thin sheets into 3-D shapes often requires less material than an equivalent solid structure. There are many planar fabrication techniques, such as laser cutting and lithography, that can be used to create composites more quickly and inexpensively than 3-D printing. Additionally, foldable machines can be transported in their two-dimensional form to ease logistics,[7,8] and folded beams and corrugated composites can achieve better stiffness-to-weight ratios than solid material. Folding is capable of creating arbitrarily

complex shapes,[9–12] mechanisms,[13–18] and even robots.[4,5,19,20] Unfortunately, as these machines become more complicated, manually folding them requires greater skill and effort. Even a simple printable robot, for example, can require more than 100 folds,[5] and at small scales manual folding becomes impossible.

Self-folding structures enhance the value of this fabrication method by reducing the time and effort required to assemble complex geometries. They also allow structures to be folded remotely and autonomously, potentially reducing human exposure to hostile environments: flat satellites could be folded after reaching orbit,[7] or military structures could be assembled without engineers present. There are a diverse range of self-folding techniques that have already been demonstrated.[21] These methods utilize heat,[22–25] magnetic fields,[26,27] electric fields,[28] or liquid[29,30] to trigger folding along hinges. However, each has one or more limitations. Some can only fold simultaneously because they rely on global stimuli, such as shape memory polymers (SMPs) heated by light absorption;[22] this precludes any structure which must be folded sequentially. Others require infrastructure such as lasers to trigger folding,[23] increasing manufacturing costs and limiting the self-folding process to specialized facilities. Many stimuli also require line-of-sight,[22,23] making some hinges difficult to actuate due to occlusion. Finally, some methods have achieved localized and sequential self-folding, but this is accomplished with discrete actuators at each hinge and component assembly, making the method costly and time consuming.[31]

We have developed a novel method for self-folding that is localized, sequential, inexpensive, and functional. This technique can be used to create a wide range of three-dimensional structures, three of which are shown below. It is well-suited to both mass

[a]*School of Engineering and Applied Sciences, Harvard University, 60 Oxford st, Cambridge, MA, 02138, USA. E-mail: sam@seas.harvard.edu; Tel: +1 617-384-7892*

[b]*Department of Mechanical Engineering, Worcester Polytechnic Institute, 100 Institute rd, Worcester, MA, 01609, USA*

[c]*Department of Electrical Engineering and Computer Science, Massachusetts Institute of Technology, 32 Vassar st, Cambridge, MA, 02139, USA*

manufacturing and low-batch production because it relies on rapid and inexpensive fabrication techniques. These features, combined with appropriate control and computation algorithms, would enable the broad use of self-folding for rapid and easy fabrication of three-dimensional devices using printing processes.

This method utilizes composites of SMP bonded to paper and activated by joule heating *via* resistive circuits.[20] SMPs are polymers that transition from a glass to a rubber phase when heated above their transition temperature, resulting in a pro-grammed shape change.[32,33] In this application, we used flat sheets of polyolefin (PO) that shrink uniaxially, and sheets of polystyrene (PS) that shrink biaxially. Both materials contract by 50% when heated above their transition temperature $T_g = 95$ °C. When this contractile layer is bonded to a passive substrate such as paper, it forms a bimorph actuator; contraction of the SMP layer causes the composite to bend. This bending can be localized at a hinge by weakening the substrate along a line, resulting in a fold (Fig. 1). The composite can be assembled cheaply by laser-cutting each layer separately, then bonding them together and aligning with pins (Fig. 2). Resistive circuits at each hinge are included on a separate layer of polyimide to induce localized SMP contraction *via* joule heating. This layer is flexible, and has minimal impact on the mechanics of the composite. Folds can be activated simultaneously or sequen-tially by applying a current to the appropriate circuit. Each layer is bonded with silicone tape.

In this paper we treat the hinges as ideal bimorph actuators and estimate their torque and displacement. A model of hinge torque was developed in order to deduce design rules for the hinges. We then designed and built test hinges and measured their temperature, torque, and displacement while varying three hinge characteristics: the thickness of the SMP layer t_{smp}, the trace width w_{trc}, and the current I (Fig. 2). For each sample we measured blocked torque and free displacement as a func-tion of current and time. Blocking was achieved *via* a mass hooked into the hole on one face of the hinge, acting as a point load.
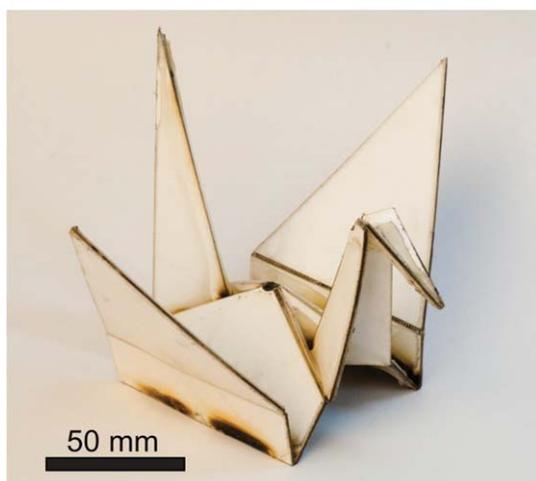
Fig. 1 An origami-inspired self-folding crane. This structure began as a two-dimensional composite of paper, prestretched polystyrene, and a copper circuit etched onto polyimide. Joule heating resulted in self-folding in three minutes.
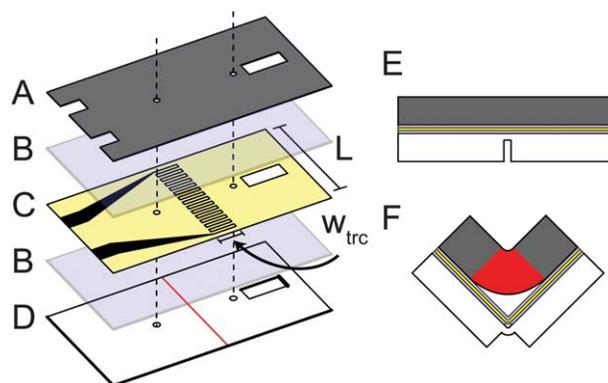
Fig. 2 (A–D) The self-folding composite samples used in the characterization experiments are assembled from three separate layers and bonded with silicone tape. (A) The PO SMP layer has notches along the bottom edge to expose copper pads. (B) Each layer is bonded to the next with 50 μm silicone tape. (C) The copper trace is 0.5 mm wide and 18 μm thick, and consists of a serpentine pattern to maximize heat dissipation. The trace is etched onto a 12 μm thick polyimide sheet. (D) The substrate is 510 μm (20 mil) paper, scored along the hinge in the middle. (E and F) Upon activation, the SMP contracts, causing the composite to bend at the hinge.

2 Model

In order to predict the hinge torque, we developed a two-part model: a thermal component considers the energy that trans-forms the SMP from a glass to a rubber phase, and therefore how much of the material is under stress, and a mechanical component correlates stress in the SMP to torque around the hinge. As a hinge folds, the lever-arm of the SMP layer on each side increases; therefore, the hinge torque is weakest when the fold is flat. Thus we use this configuration as a "worst-case" scenario for our models (Fig. 3A). Once a hinge begins to fold, the increased lever arm will cause it to continue folding until the stress is relieved. Additionally, during the folding process, the SMP delaminates from the circuit; this affects the thermo-dynamics of the system, but when the hinge is held flat, the change is negligible.

2.1 Thermal model

The hinge is close to isothermal in the *y*- and *z*-directions (ESI†); we therefore treat the thermal system as one-dimensional. The SMP layer is modeled as two adjacent but distinct regions: the core consists of all material directly above the electrical trace, and the margin is all material outside of the core. The marginal area is considered to be a semi-infinite region extending away from the hinge, $x \rightarrow \infty$, while the core is equivalent to the surface at $x = 0$ (Fig. 3). We can therefore treat the convection and heat generation occurring in the core to be at the surface of our semi-infinite material. By modifying the solution to a related problem,[34] the temperature is calculated as

$$T(x,t) - T_o = \frac{q_{gen}}{h'}\left[\text{erfc}\left(\frac{x}{2\sqrt{\alpha t}}\right)\right.$$

$$\left. - \exp\left(\frac{h'x}{k} + \frac{h'^2\alpha t}{k^2}\right)\text{erfc}\left(\frac{x}{2\sqrt{\alpha t}} + \frac{h'\sqrt{\alpha t}}{k}\right)\right] \quad (1)$$
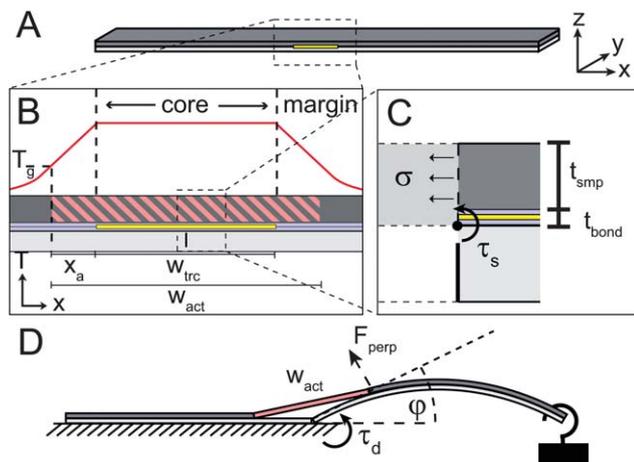
Fig. 3 (A) The model predicts the hinge torque of the composite in a flat state. (B) The thermal component assumes a uniform temperature in the core, and a semi-infinite transient solution in the margin. The material above the transition temperature T_g, indicated by the striped region, extends out to the limit x_a, covering a total length w_{act}. (C) A free body diagram of one side of the hinge, indicating the static torque τ_s around the hinge point due to the stress at the midplane. (D) The deformed mechanical component determines the additional torque τ_d from an increased lever-arm when the hinge bends, such as the when a blocking force is applied, via a hanging weight, to the face during testing. The deformation in this figure is exaggerated.

where erfc is the complementary error function, T_o is the ambient temperature, k is the SMP thermal conductivity, α is the SMP thermal diffusivity, x is the distance from the core region, t is time, q_{gen} is the specific power generated by the resistive circuit, and h' is the time-dependent heat transfer coefficient (ESI†). h' takes into account several parameters: the surface heat transfer coefficient h_{smp}, the ratio of heated surface area to the cross-sectional area material, and the fact that this heated surface area is expanding.

$$h' = \frac{h_{smp} w_{trc}}{2(t_{smp} + w_{trc})}\left(1 + \frac{\sqrt{\alpha t}}{w_{trc}}\right) \qquad (2)$$

The derivation of eqn (1), as well as values for these constants for the case of a test hinge with a 560 µm (22 mil) SMP layer being supplied with two amperes of current, are shown in the ESI.†

We use this model to determine the region, defined by the distance x_a from the core, of the material that is above the transition temperature. x_a is approximated by finding the first-order Taylor expansion of $T(x,t)$ around $x = 0$. This is used to calculate the total length of activated SMP, $w_{act} = w_{trc} + 2x_a$.

When comparing this model to thermal data, one additional factor is included. While the change in the SMP temperature in the z direction is not great enough to alter the model, there is a noticeable decrease in the temperature at the surface due to the thermal resistance of the SMP. To compensate, the model is multiplied by a coefficient C_s representing the relationship between the inner temperature of the SMP and the surface temperature $T_s = C_s T$ (ESI†). In our samples, C_s was never less than 0.9. Because our experiments measure the surface

temperature of the SMP, this factor is included when comparing the model to thermal data.

2.2 Mechanical model

In order to determine the hinge torque, we consider the SMP to be a plane-strain problem, so that the stress in the x-direction $\sigma = 4E\varepsilon/3$ at the midplane of the hinge $x = 0$, where E is the Young's modulus of the SMP in its rubber state (assumed to be constant) and ε is the strain of the SMP in the x-direction. At room temperature, this stress and strain are uniformly zero. However, as the material temperature exceeds the transition temperature, the effective strain in the material becomes equal to one. We use the estimate from Tobushi *et al.* that the material transition occurs linearly over a 30 °C temperature range so that:

$$\varepsilon = \frac{T(0,t) - T_g + 15}{30} \qquad T_g - 15 < T(0,t) < T_g + 15 \qquad (3)$$

This strain correlates with a stress, which in turn results in a torque τ_s around the pivot point of the hinge (Fig. 3C). This pivot point is assumed to be at the interface between the substrate and the adhesive.

$$\tau_s = \frac{4LE\varepsilon}{3}\frac{\left(t_{smp}^2 + 2t_{smp}t_{bond}\right)}{2} \qquad (4)$$

where t_{bond} is the combined thickness of the copper–polyimide and the silicone tape.

However, there is additional torque resulting from deformation of the hinge (Fig. 3D). When the hinge experiences torque, a reactive force is often exerted on one or both hinge faces by gravity or physical interference. Specifically, in our experimental setup there is a point load at the end of one hinge face that balances the hinge torque in order to measure the blocked torque. This point load causes the hinge face to bend, similar to a cantilevered beam, resulting in a small displacement angle $\phi = \tau/I_b$, where I_b is the stiffness of the face, and τ is the total torque. As mentioned above, any non-zero angle will increase the torque by increasing the lever-arm, and this increase is modeled as a separate torque τ_d, as if the activated SMP of length w_{act} were in uniform tension and straight from one face to another at an angle of $\phi/2$.

$$\tau_d \approx \frac{\sigma L t_{smp} w_{act} \phi}{4} \qquad (5)$$

By substituting $\tau = I_b\phi$ and $\tau = \tau_s + \tau_d$, we calculate

$$\tau \approx \frac{2ELI_b\left(t_{smp}^2 + 2t_{bond}t_{smp}\right)}{3I_b - ELt_{smp}w_{act}} \qquad (6)$$

3 Results and discussion

We measured the core temperature $T(0,t)$ of hinge actuators with 690 µm (27 mil) thick SMP layers, when their heating circuits were supplied with both 2 and 1.75 A (Fig. 4A). The data indicates that our model is effectively predicting the temperature of the hinge. The temperature was measured for hinges
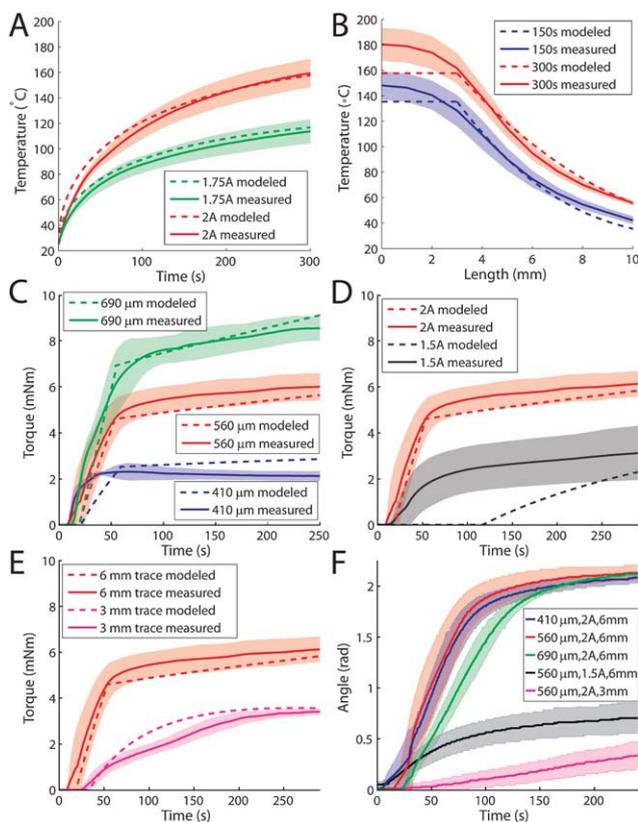
Fig. 4 (A) The measured and modeled core temperature T of a hinge with a 690 µm SMP layer when either 1.75 or 2 A were supplied, as a function of time. (B) The measured and modeled temperature profile T of a hinge with a 690 µm SMP layer after two amperes were supplied for 150 s or 300 s, as a function of distance from the hinge center. (C–E) The measured and modeled torque exerted by hinges with SMP thicknesses of 410 µm, 560 µm, 690 µm when supplied with two amperes (C), with a 560 µm SMP layer when supplied with 1.5 or 2 A (D) and when the trace is six millimeters wide or three millimeters wide (E). (F) The displacement of an unloaded hinge face for SMP thicknesses of 410 µm, 560 µm, and 690 µm with a six millimeter trace supplied with 2 A, as well as a 560 µm thick SMP with a six millimeter trace at 1.5 A, and with a three millimeter trace at 2 A. Five samples per set were used for the thermal and torque measurements, and three samples per set were used for displacement measurements. The shaded area indicates the standard deviation of the data over time.

with a 410 µm (16 mil) thick SMP layer as well, and both the model and the measurements indicate that SMP thickness has a small effect on the surface temperature. The model predicts that the measured surface temperature of the hinge with 690 µm SMP will always be 9% less than the hinge with 410 µm SMP. Measured temperatures supported this calculation; after the first minute of activation, the measured temperature of the 690 µm SMP remained within 10% of the temperature of the 410 µm SMP. The predicted difference in T_s between the two thicknesses is derived solely from the difference in C_s between the models; the model predicts identical inner temperatures for the two hinge designs.

We measured the temperature profile of the SMP as a function of distance from the hinge line (Fig. 4B). In the margin, the model closely resembles the measured temperature, indicating that the semi-infinite assumption is appropriate.

We measured and compared the blocked torque exerted by hinges with SMP thicknesses of 410 µm (16 mil), 560 µm (22 mil), and 690 µm (27 mil) when activated by two amperes and held in a flat configuration (Fig. 4C). The torque exhibits two regimes. The first, characterized by a rapid increase in torque and lasting approximately 50 seconds, is governed by the rise in core temperature, until the material in the core has surpassed the transition temperature. The second regime embodies a steady or slowly increasing torque, governed by deformations occurring in the hinge face. At 560 and 690 µm, the experiments match the model assumptions of slowly increasing deformation, resulting in both a larger initial torque during the first regime, and a slow increase in torque during the second. At 410 µm, the experiment does not exhibit any growth in the second regime, and instead resembles the model without deformation; it is possible that the torque exerted from the 410 µm SMP is not large enough to cause deformation.

The torque was also measured for hinges with 560 µm SMP at 1.5 A, and with a three millimeter wide trace. In the case of a reduced current, the model and the experiments both indicate a lower torque that builds more slowly (Fig. 4D). At 1.5 A, torque is measured earlier than the model would predict. We believe this is due to discrepancies between our model of the SMP transition regime and reality; our model uses a linear assumption of the material transition, which is sufficient when the SMP temperature increases rapidly through the transition regime. In the case of a reduced current with a slower temperature rise, the differences become more apparent.

When the trace width was reduced to three millimeters, the model accurately predicts a decrease in torque (Fig. 4E). The trace width affects the torque by two means: a reduced trace produces less heat, slowing the SMP transition, and the small core leads to a smaller active width, reducing the deformation torque.

Folding displacement was characterized by observing the fold angle of a hinge as a function of time when supplied with a set current. One face of the hinge was constrained to a horizontal surface while the other was unrestrained. As can be seen in Fig. 4F, the SMP thickness has no effect on displacement. However, decreasing the current to 1.5 A or decreasing the trace width to three millimeters causes a significant decrease in displacement. We believe this difference is related to the hinge geometry as it folds. When the SMP begins to contract, it delaminates from the resistive circuit, reducing the heat flux into the SMP. When the trace size or the current is reduced, it reduces the total energy produced, and so reduces the distance that the SMP can depart from the trace before dropping below the transition temperature. When the SMP exceeds this distance, folding stops, resulting in a limit on displacement.

One interesting behavior is that the hinges often bend slightly ($\approx 5°$) in the opposite direction before folding. We believe this is due to expansion of the SMP as its temperature increases, but before it transitions into a rubber state.

Because our interest is in developing design rules for utilizing this self-folding method, we used our model to explore how different variables affected hinge torque. While the effect of t_{smp} on torque is apparent from both the model and the
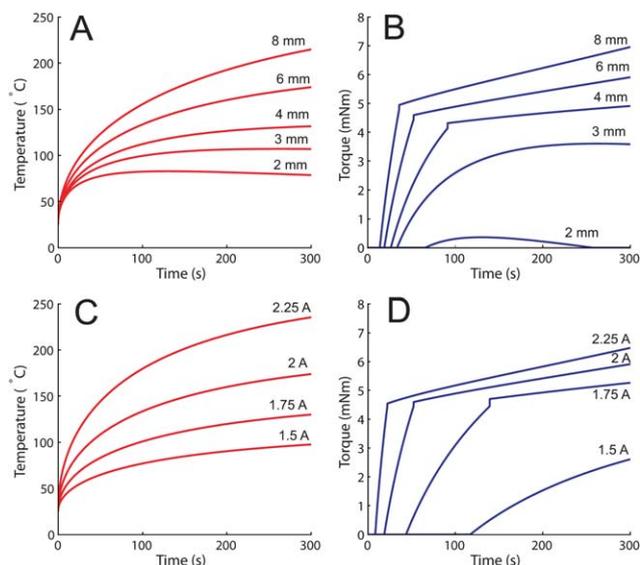
Fig. 5 Simulations were run of a hinge with $t_{smp} = 560$ μm, $I = 2$ A, and a range of values for w_{trc}; the resulting core temperature (A) and torque (B) are shown above. A critical trace width was observed, corresponding with the complete activation of the core. More simulations were run with a fixed $w_{trc} = 6$ mm and a range of values for I. The core temperature (C) and torque (D) indicate there is a critical value for the current, below which torque decreases significantly.

experiments, the effects of other variables are more complicated. We therefore simulated the hinge torque for a range of currents, and then for a range of trace widths (Fig. 5). In both cases, increasing the value of these variables always increased torque, but there was a critical value for each, below which torque fell off significantly, and above with torque increased

slowly. For w_{trc}, this critical value corresponds with the complete activation of the core region, $T(0,t) = T_g + 15$ K. If w_{trc} is too small, the growth of convective heat loss outpaces resistive heat generation before the core fully activates, significantly limiting the torque.

Current affects torque by increasing the magnitude of the temperature T. While the model predicts that $T(0,t)$ will continue to grow at all times as long as w_{trc} is sufficient, there is an inflection point at which this growth slows. We can calculate a minimum recommended current I_r so that $T(0,t^*) = T_g$ by the time t^* the inflection point is reached.

$$I_r = \sqrt{\frac{(T_g - T_o)(h_{smp}w + k)L}{0.57R}} \tag{7}$$

Using the values for this hinge (Table 1 in ESI†), we find $I_r = 1.6$ A, which is consistent with our simulations. In addition, there is an effective upper limit to the appropriate range of current used for self-folding. If the SMP is heated to its melting point, the Young's modulus will decrease significantly, reducing torque and limiting displacement. Therefore, the current must be set so that the SMP stays between its glass transition temperature and its melting temperature. This temperature varies greatly depending on the material used, but was never reached in our experiments.

In order to demonstrate the functionality and versatility of these composites, we built three self-folding structures using PS as a biaxial SMP layer to actuate non-parallel folds (Video S1†). We constructed a self-folding pyramid, seen in Fig. 6A and B, to demonstrate concurrent folding into a polyhedron. The four folds were simultaneously activated by linking the resistive circuits in series. We also built a self-locking slot-and-tab
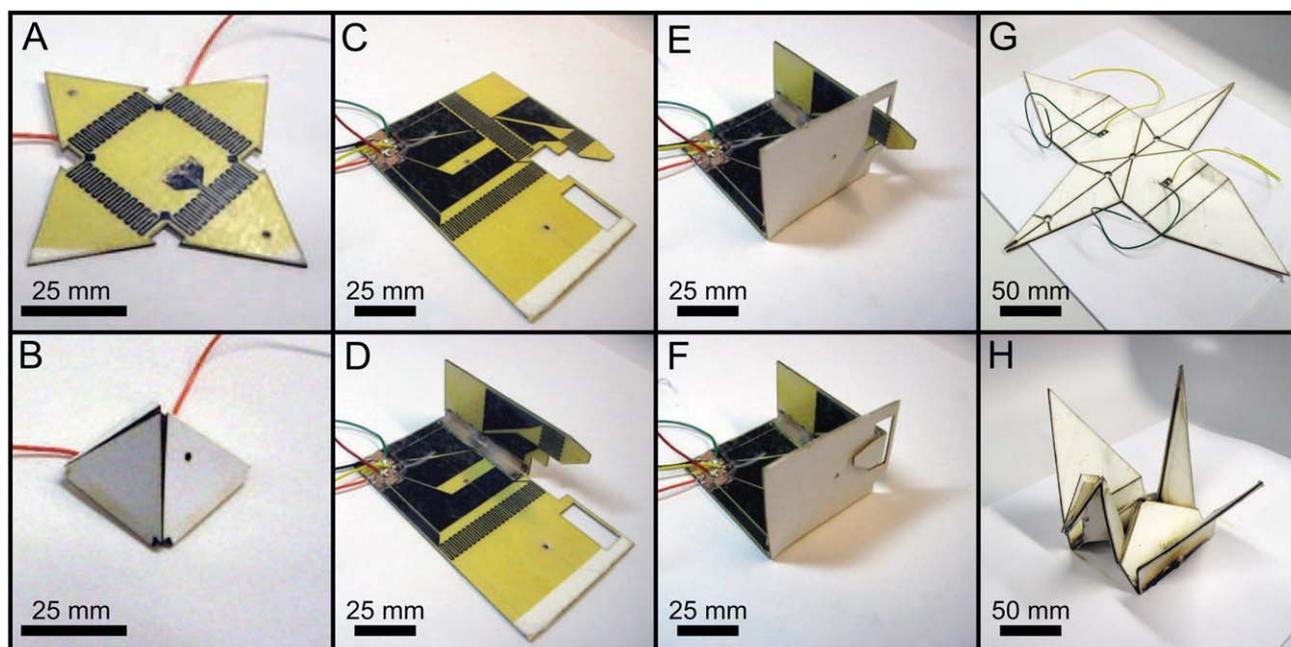
Fig. 6 (A and B) A pyramid folded through simultaneous activation of four hinges *via* two amperes supplied to a series of resistive circuits. (C–F) A locking slot and tab assembly. This fold is only possible with sequential folding. (G and H) A crane, created with a combination of sequential and simultaneous folding.

assembly, seen in Fig. 6C–F. This mechanism locked by first actuating the folds to fit the slot into the tab, and then actuating another hinge within the tab to hold the slot in place. This mechanism demonstrates the efficacy and potential applications of sequential folding. A more complex structure consisting of 15 active and 4 passive hinges was designed to assemble into a crane (Fig. 6G and H). This composite consisted of two layers of paper and two layers of PS sandwiching the circuit layer in order to actuate both mountain and valley folds. Two amperes of current were first supplied to all hinges except the two most distal wing hinges, causing the body to fold. Once it had folded, two amperes were supplied to the remaining distal hinges to bring the wings down. In each structure, individual folds were activated with two amperes for one to two minutes, so that all examples completed their self-folding in less than four minutes (Video S1†). These examples also demonstrated the speed they could bring to printable manufacturing. The crane (Fig. 6G and H), for example, took approximately one hour to assemble by hand, using only a laser cutter, a solid ink printer, and a ferric chloride etch tank.

This technique still has limitations that prevent it from achieving any theoretically possible folded shape; these limitations include the composite thickness, hinge torque, maximum fold angle, and material resolution. However, with the development of appropriate materials, we believe that all of these characteristics can be improved. Furthermore, there are many possible applications for this technique that can still be explored. Due to the nature of current as a stimulus, self-folding structures could be triggered remotely, or even control their own activation through integrated circuits. The extra weight for autonomous assembly would be minimal; a ProTek R/C "High Power" 1S Li–Po battery pack can provide 300 mA h, more than enough to fold the crane, while weighing eight grams. High volume assembly could also be an application for self-folding, as this technique lends itself to inexpensive construction in parallel. Finally, the automated nature of this technique suggests it could be applied to mesoscale manufacturing problems, similar to Pop-Up Book MEMS.[18,19] Self-folding with shape memory composites provides speed and automation for origami-inspired fabrication, which in turns offers a faster and more efficient alternative to 3-D printing and traditional manufacturing.

4 Experimental

4.1 Test hinges

Test hinges for all experiments were 30 mm wide. One face was 30 mm long with copper pads at the bottom edge, and was intended to be immobile during tests. The other face was 27 mm long, with a slot near the far edge designed to fit a weighted hook for torque testing. This slot was positioned so that the hook applied a point load 25 mm from the hinge. Each composite consisted of a 510 μm sheet of paper (Cold Press Bright, Epson), an 18 μm layer of polyimide with a 12 μm copper resistive circuit (AC181200R, DuPont), and a layer of PO of varying thickness. The resistive circuit trace was 0.5 mm wide, and consisted of a serpentine pattern with segments one millimeter apart and of length w_{trc} that varied between experiments. The PO was extracted from

heat shrink tubing (16 mil: RNF-100-1-BK-STK; 22 mil: RNF-100-2-BK-STK; 27 mil: TAT-125-2-0; Raychem). Each layer was bonded with double-sided, 50 μm thick silicone tape (ARclad 7876, Adhesives Research). Each layer was cut using a commercial C02 laser machining system (VLS 2.3, Universal Laser Systems), and the copper circuit was etched with ferric chloride, masked by a solid ink printer (Colorqube, Xerox).

4.2 Thermal measurements

Both faces of the test hinge were secured to a horizontal piece of acrylic to maintain a flat state. A set amount of current was supplied to the resistive circuit, and the SMP surface temperature was measured with a thermal camera (T440, FLIR) at a rate of two hertz for six minutes. The core temperature was determined by averaging the surface temperature over the area above the trace, and the marginal temperature was determined from the temperature profile along the midline of the SMP, perpendicular to the hinge (Fig. 7). Five samples were used for each experiment.

4.3 Blocked torque measurements

Each sample was positioned so that the hinge was held flat and blocked by a weight hooked through the slot on the 27 mm hinge face. This weight rested on a scale (PL 303, Mettler Toledo). The 30 mm side of the sample was secured to a horizontal piece of acrylic with tape, and either 2 or 1.5 A was supplied to the resistive circuit for five minutes. When folding was triggered, the sample exerted a force on the weight to balance the hinge torque. The torque was deduced from the change in weight registered by the scale, indicating the point load applied on the hinge face by the weight. Data was collected with Matlab *via* a serial cable at approximately 8.3 Hz. Five samples were used for each experiment.

4.4 Free displacement measurements

The 30 mm face of the hinge was secured to a horizontal piece of acrylic, and a fixed amount of current was supplied to the resistive circuit for 5 minutes. The process was recorded using a camera (Powershot A1100 IS, Canon), and the angle between the moving face and the horizontal surface was determined *via* image processing at half-second intervals. Three samples were used for each experiment.
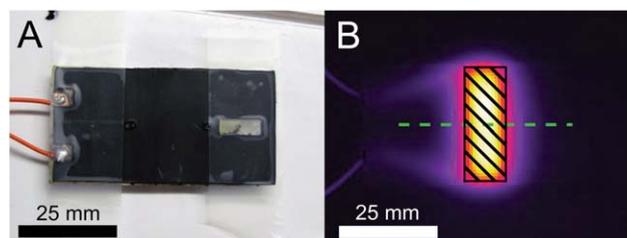
Fig. 7 The experimental setup used to measure the hinge SMP temperature, viewed in the visual spectrum (A), as well as through a thermal camera (B). The core temperature was determined by averaging the temperature of each pixel within the striped box. The marginal temperature was determined by measuring the temperature profile along the dashed line.

4.5   Young's modulus measurements

A 25 mm wide by 15 mm long strip of 410 μm thick polyolefin was heated above 120 °C *via* joule heating from a flexible circuit. While heated, it was stretched at a rate of 500 μm s^{-1} to a final length of 30 mm in a mechanical testing machine (5566, Instron). During this time the resulting force was measured at 20 Hz. The force was found to be approximately linearly proportional to the displacement over the range measured, and the Young's modulus in the rubber state was determined to be 400 kPa from the ratio of the engineering stress to the strain.

Acknowledgements

References

1 J. A. Lewis and G. M. Gratson, *Mater. Today*, 2004, **7**, 32–39.
2 K. Willis, E. Brockmeyer, S. Hudson and I. Poupyrev, *Proceedings of the 25th annual ACM symposium on user interface software and technology*, 2012, pp. 589–598.
3 B. ONeill, *Inkjet Technology for Digital Fabrication*, 2012, pp. 325–342.
4 C. D. Onal, R. J. Wood and D. Rus, *IEEE Int. Conf. on Robotics and Automation (ICRA)*, 2011, pp. 4608–4613.
5 C. D. Onal, R. J. Wood and D. Rus, *IEEE ASME Trans. Mechatron.*, 2012, **18**, 430–438.
6 B. Y. Ahn, D. Shoji, C. J. Hansen, E. Hong, D. C. Dunand and J. A. Lewis, *Adv. Mater.*, 2010, **22**, 2251–2254.
7 K. Miura, *31st Congress of the International Astronautical Federation*, 1980.
8 R. Konings and R. Thijs, *Eur. J. Transport. Infrastruct. Res.*, 2001, **1**, 333–352.
9 E. D. Demaine, M. L. Demaine and J. S. B. Mitchell, *Comput. Geom.*, 2000, **16**, 3–21.
10 E. D. Demaine and M. L. Demaine, *Proceedings of the 3rd International Meeting of Origami Science, Math, and Education*, 2001, pp. 3–16.
11 J. Mitani, *Comput. Aided Des. Appl.*, 2009, **6**, 69–79.
12 S. Pandey, M. Ewing, A. Kunas, N. Nguyen, D. H. Gracias and G. Menon, *Proc. Natl. Acad. Sci. U. S. A.*, 2011, **108**, 19885–19890.
13 E. M. Arkin, S. P. Fekete and J. S. B. Mitchell, *Comput. Geom.*, 2003, **25**, 117–138.
14 H. Okuzaki, T. Saido, H. Suzuki, Y. Hara and H. Yan, *J. Phys.: Conf. Ser.*, 2008, 012001.
15 C. C. Min and H. Suzuki, *Manufacturing Systems and Technologies for the New Frontier*, 2008, pp. 159–162.
16 K. Kuribayashi, K. Tsuchiya, Z. You, D. Tomus, M. Umemoto, T. Ito and M. Sasaki, *Mater. Sci. Eng., A*, 2006, **419**, 131–137.
17 X. Guo, H. Li, B. Y. Ahn, E. B. Duoss, K. J. Hsia, J. A. Lewis and R. G. Nuzzo, *Proc. Natl. Acad. Sci. U. S. A.*, 2009, **106**, 20149–20154.
18 J. Whitney, P. Sreetharan, K. Ma and R. Wood, *J. Micromech. Microeng.*, 2011, **21**, 115021.
19 P. Sreetharan, J. Whitney, M. Strauss and R. Wood, *J. Micromech. Microeng.*, 2012, **22**, 055027.
20 S. Felton, M. Tolley, C. D. Onal, D. Rus and R. J. Wood, *IEEE Int. Conf. on Robotics and Automation (ICRA)*, 2013, pp. 277–282.
21 L. Ionov, *Soft Matter*, 2011, 6786–6791.
22 Y. Liu, J. K. Boyles, J. Genzer and M. D. Dickey, *Soft Matter*, 2012, **8**, 1764–1769.
23 K. E. Laflin, C. J. Morris, T. Muqeem and D. H. Gracias, *Appl. Phys. Lett.*, 2012, **101**, 131901.
24 G. Stoychev, N. Puretskiy and L. Ionov, *Soft Matter*, 2011, **7**, 3277–3279.
25 J. Kim, J. A. Hanna, R. C. Hayward and C. D. Santangelo, *Soft Matter*, 2012, **8**, 2375–2381.
26 J. W. Judy and R. S. Muller, *J. Microelectromech. Syst.*, 1997, **6**, 249–256.
27 Y. W. Yi and C. Liu, *J. Microelectromech. Syst.*, 1999, **8**, 10–17.
28 M. Piñeirua, J. Bico and B. Roman, *Soft Matter*, 2010, **6**, 4491–4496.
29 J. Guan, H. He, D. J. Hansford and L. J. Lee, *J. Phys. Chem. B*, 2005, **109**, 23134–23137.
30 W. Li, G. Huang, H. Yan, J. Wang, Y. Yu, X. Hu, X. Wu and Y. Mei, *Soft Matter*, 2012, **8**, 7103–7107.
31 E. Hawkes, B. An, N. M. Benbernou, H. Tanaka, S. Kim, E. D. Demaine, D. Rus and R. J. Wood, *Proc. Natl. Acad. Sci. U. S. A.*, 2010, **107**, 12441.
32 A. Lendlein and S. Kelch, *Angew. Chem., Int. Ed.*, 2002, **41**, 2034–2057.
33 A. Lendlein, H. Jiang, O. Jünger and R. Langer, *Nature*, 2005, **434**, 879–882.
34 F. P. Incropera and D. P. Dewitt, *Fundamentals of heat and mass transfer*, 5th Edition, 2002, pp. 268–271.